Role of He excited configurations in the neutralization of He^+ ions colliding with a HOPG surface

A. Iglesias-García,[1,2] Evelina A. García,[1] and E. C. Goldberg[1,3]

[1]*Instituto de Desarrollo Tecnológico para la Industria Química (INTEC-CONICET-UNL) Güemes 3450, CC91, (S3000GLN) Santa Fe, Argentina*

[2]*Facultad de Humanidades y Ciencias, Universidad Nacional del Litoral, Santa Fe, Argentina*

[3]*Departamento de Ingenieria de Materiales, Facultad de Ingenieria Química, U.N.L., (S3000GLN) Santa Fe, Argentina*

(Received 15 October 2012; revised manuscript received 15 January 2013; published 22 February 2013)

The very high neutral fractions measured in He^+ scattered by graphitelike surfaces, at intermediate incoming energies (1 keV $< E_{in} <$ 6 keV), cannot be explained only by the resonance of the He ionization level with the valence band states of the surface. Excited configurations ($1s2s$) and ($1s2p$) appear as possible resonant neutralization channels together with the ground state one ($1s^2$). We develop, in this work, a time-dependent quantum-mechanical calculation of the charge-transfer process in He^+/HOPG collision, where the resonant neutralization to the ground and first excited states of He is taken into account. We use an Anderson Hamiltonian projected on the electronic configurations of the projectile atom which are energetically favorable for the charge-exchange process. Thus, an exhaustive analysis of different possible approximations to the neutralization of He^+ is performed: the typical neutralization to the ground state by either neglecting or not the electron spin and finally the one including excited configurations. Our results reproduce the observed experimental trends only when excited configurations ($1s2s$) and ($1s2p$) are involved in the charge exchange between the ion and the surface.

DOI: 10.1103/PhysRevB.87.075434 PACS number(s): 34.70.+e, 34.35.+a, 68.43.−h, 68.49.Sf

I. INTRODUCTION

The inelastic interaction of low-energy ions with surfaces is a very complex process which depends strongly on the characteristics of the electronic structure of both surface and ion. It is, on the other hand, the basis of an important surface characterization technique, *low energy ions spectrometry*, being the quality of this specific technique determined by the balance of the different neutralization mechanisms involved. The relevant mechanisms are resonant, Auger, and collision induced processes.[1]

Resonant processes proceed via electron tunneling between target conduction band and bound states of the projectile; their probabilities depend strongly on the distance surface projectile and on the binding energies of the involved levels. In a resonant transition only one electron is involved; therefore the corresponding transition rates (i.e., the probability for a resonant transition per time unit) are, within linear theory, proportional to the density of involved electronic states which is commonly assumed to be high. Thus, resonant processes are considered to be dominant whenever they are possible.[2–9]

Many different Auger processes contribute to the Auger neutralization (AN)[10] mechanism: direct AN of the incoming ion to the ground state by a metal electron, with excitation of another metal electron or a plasmon; direct Auger deexcitation, where a metastable atom is first formed by tunneling of a metal electron to an excited state, which then decays to the ground state, with excitation of a metal electron or a plasmon; and finally, indirect Auger deexcitation, where a metal electron fills the hole in the inner state of the excited atom, with emission of the electron of the outer level of the atom.[11–20]

It has been shown by *ab initio* Hartree-Fock calculations that collision induced neutralization (reionization) can be caused by level crossings of the He($1s$) level with occupied (empty) conduction levels of the target, as a consequence of the antibonding interaction of the He($1s$) level with target core levels.[21]

The scattering of He^+ by an Al surface provides a good example of a case in which the neutralization occurs due to Auger and collision induced processes.[22,23] Since the helium ionization level falls below the bottom of the Al valence band, the Auger process was expected to be the only efficient neutralization mechanism. But it was found that the ion level shift due to the short-range interactions between nuclei and electrons allows a significant overlap with Al($2p$) core electrons at a distance of about 2 a.u. In this form the He($1s$) level is promoted so high that it becomes resonant with the band states, making the charge exchang possible.

An interesting case is the He^+ scattering by HOPG (*highly oriented pyrolytic graphite*), where a practically full neutralization is observed.[24–26] The wide valence band of HOPG makes the resonance with the He-$1s$ level possible, therefore it is expected that the resonant process dominates in comparison with the Auger process. No collision induced processes are expected in this system because of the large binding energy of the target core level, C-$1s$, and the much localized nature of this inner state. It has been stated that resonant neutralization to the first excited level of the noble gas ions is only possible for low-work-function metals, its extent depending on the ionization potential of the first excited level and the velocity of the ion.[27] There is, however, new experimental evidence showing that ion neutralization at clean, high-work-function metal surfaces occurs at much smaller ion-surface separations than inferred from earlier measurements of ion scattering. Thus, through the strong short-range chemical interactions between incident ion and neighboring metal atoms, the energy level shifts should be more important than previously thought.[28,29] Very preliminary results[26] showed that the significant neutralization observed in He^+/HOPG can only be reproduced theoretically by considering excited states of the neutral He atom. This calculation was performed by using an infinite-correlation approach to the Anderson Hamiltonian[30] and by considering, within a simplified picture, the spin component of the first electron in He^+ frozen. Thus, a second electron with the

same spin component is responsible for the neutralization to the excited state $(1s\uparrow 2s\uparrow)$, while a second electron with the opposite spin component is responsible for the neutralization to the ground state $(1s\uparrow 1s\downarrow)$. A neutral fraction of 95% was measured in backscattering conditions and for incoming ion energy equal to 5 keV, while the calculation predicted a neutral fraction of 85% when including the excited state He$(1s2s)$ and of 35% when only the ground state He$(1s^2)$ was considered.

In the present work we present an exhaustive study of the resonant neutralization of positive helium ions in the scattering by a HOPG surface. First, we performed an analysis of the most probable atomic configurations to be included as possible neutralization channels. Then, the Anderson-like Hamiltonian is projected over this configuration space. In this way, the ion neutralization is calculated by considering the ground state and excited states $(1s2s)$ and $(1s2p)$ as probable channels of charge exchange between the ion and the surface. The spin fluctuation statistics involved in the $He^+(1s)$ to He$(1s^2)$ transition via the surface band states is also taken into account in the present theoretical proposal. The dynamical collision process is solved by using the equations of motion of the time-dependent Green functions proposed by Keldysh[31,32] which allow us to treat the interaction of electronic configurations in a correct way.

The work is organized as follows. In Sec. II we discuss the electronic configurations defining the atomic part of the Anderson Hamiltonian; then, the projection of the interaction Hamiltonian over the selected configurations, and the Green function formalism used for calculating the physical magnitudes of interest are presented. The calculation of the energy and coupling terms of the Hamiltonian is also discussed in this section. In Sec. III we discuss our obtained results by going from the simplest description of the atom-surface interaction (*spinless model*) to the improved one involving many correlated charge-transfer channels and including spin fluctuation statistics. The concluding remarks are presented in Sec. IV.

II. THEORY

The general form of our initial Hamiltonian is the following extended Anderson Hamiltonian:[33]

$$\hat{H} = \sum_{\vec{k},\sigma} \varepsilon_{\vec{k}} \hat{n}_{\vec{k}\sigma} + \hat{H}_{\text{atom}} + \sum_{\vec{k}m,\sigma} \left(\hat{V}^{\sigma}_{\vec{k}m} \hat{c}^{\dagger}_{\vec{k}\sigma} \hat{c}_{m\sigma} + \text{H.c.} \right). \quad (1)$$

The preliminary calculation of Ref. 26 based on a very rough approximation of the correlated ground and excited neutralization channels, is clearly improved in this work by correctly considering the possibility of many states in the atom through the following extended atomic Hamiltonian, which allows us to perform an interaction of configurations within the time-dependent collision process:

$$\begin{aligned} \hat{H}_{\text{atom}} = & \sum_{m,\sigma} \zeta_m \hat{n}_{m\sigma} + \sum_{m} U_m \hat{n}_{m\uparrow} \hat{n}_{m\downarrow} \\ & + \frac{1}{2} \sum_{m \neq m',\sigma} J_{mm'} \hat{n}_{m\sigma} \hat{n}_{m'-\sigma} \\ & + \frac{1}{2} \sum_{m \neq m',\sigma} \left(J_{mm'} - J^{x}_{mm'} \right) \hat{n}_{m\sigma} \hat{n}_{m'\sigma} \\ & - \frac{1}{2} \sum_{m \neq m',\sigma} J^{x}_{mm'} \hat{c}^{\dagger}_{m\sigma} c_{m-\sigma} c^{\dagger}_{m'-\sigma} c_{m'\sigma}. \end{aligned} \quad (2)$$

In Eqs. (1) and (2) $\hat{c}^{\dagger}_{\vec{k}\sigma}$ and $\hat{c}^{\dagger}_{m\sigma}$ denote the creation operators of the conduction electrons and the localized electrons in the atomic orbital m with spin σ, respectively; $\hat{n}_{\vec{k}\sigma}(\hat{n}_{m\sigma})$ is the occupation number operator for the band (atom) states. In Eq. (1), the third term is responsible for the resonant charge transfer via a tunneling process, with $\hat{V}^{\sigma}_{\vec{k}m}$ the couplings between conduction and localized electrons in the atomic orbital. In Eq. (2), U and J are the intraatomic Coulomb interactions for the localized m orbitals and J^x is the intra-atomic exchange interaction. The last term, related to spin-flip processes, restores the invariance under rotation in spin space. ζ_m accounts for the kinetic and electron-nucleus interaction terms. Hamiltonian equation (1) is solved by projecting over the selected space of electronic configurations that describe the atom states with a significant probability of occurrence.

A. Electronic configurations of the He atom that can be probable neutralization channels in the He^+ scattering by HOPG

In the following we introduce the atomic configurations which are going to be considered in the charge exchange process.

(i) $He^+(1s)$ can be neutralized to the ground state $(1s^2)$, meaning the two possible charge-spin fluctuations: $1s\uparrow \leftrightarrow 1s\uparrow 1s\downarrow$ and $1s\downarrow \leftrightarrow 1s\uparrow 1s\downarrow$. Taking into account that the one-electron energy levels result from the difference between the total energies with $N+1$ and N electrons, in this case the one-electron level energy associated with this transition is $\varepsilon_{1s} = E(1s\uparrow 1s\downarrow) - E(1s\uparrow) = E(1s\uparrow 1s\downarrow) - E(1s\downarrow)$, which is the energy of a second electron in the He(1s) orbital.

(ii) $He^+(1s\sigma)$ can be neutralized either to the excited state $(1s\sigma 2s\sigma)$ with a z component of the total spin $S_z = 1, -1$ or to the excited state $(1s\sigma 2s\bar{\sigma})$ with $S_z = 0$, each one representing two energy degenerate possibilities. The one-electron energies associated with these charge-spin fluctuations are given by $\varepsilon_{2s\sigma} = E(1s\sigma 2s\sigma) - E(1s\sigma)$, $\varepsilon_{2s\bar{\sigma}} = E(1s\sigma 2s\bar{\sigma}) - E(1s\sigma)$, which is the energy of an electron in the $2s$ orbital in the presence of one electron in the $1s$.

(iii) $He^+(1s\sigma)$ can be neutralized to the excited state $(1s\sigma 2p_i\sigma)$ with a z component of the total spin $S_z = 1, -1$, or to the excited state $(1s\sigma 2p_i\bar{\sigma})$ with $S_z = 0$, each one representing two degenerate possibilities $(p_i = p_x, p_y, p_z)$. The one-electron energies associated with these charge-spin fluctuations are given by $\varepsilon_{2p\sigma} = E(1s\sigma 2p_i\sigma) - E(1s\sigma)$, $\varepsilon_{2p\bar{\sigma}} = E(1s\sigma 2p_i\bar{\sigma}) - E(1s\sigma)$, which is the energy of an electron in the orbital $2p_i$ in the presence of one electron in the orbital $1s$.

The atom energy and the hopping terms are obtained from a model Hamiltonian for the atom-surface adiabatic interaction based on both the localized atom-atom interactions and the extended features of the surface states.[34] A linear combination of atomic orbitals $\phi_i(\vec{r} - \vec{R}_s)$ (LCAO) is used for expanding the states of the surface, and a mean-field approximation of the two-electron interaction terms is performed. In this form, the variation with the distance to the surface of the one-electron energy levels, which correspond to the atom charge fluctuations (i)–(iii), is determined by the following short-range interaction terms (here the charge states of the atoms

are frozen to their values for the noninteracting situation):

$$\tilde{\varepsilon}_m = \varepsilon_m^0 - \sum_{\vec{R}_s} V_{m,m}^{Z_s,\vec{R}_s} + \sum_{i,\vec{R}_s} \left(2\tilde{J}_{m,i\vec{R}_s} - J^x_{m,i\vec{R}_s}\right)\langle n_i\rangle - \sum_{i,\vec{R}_s} S_{m,i\vec{R}_s} V^{\rm dim}_{m,i\vec{R}_s} + \frac{1}{4}\sum_{i,\vec{R}_s} S^2_{m,i\vec{R}_s}\Delta E_{m,i\vec{R}_s}. \quad (3)$$

In Eq. (3), ε_m^0 are in each case equal to the Hartree-Fock orbital energies ε_{1s},$\varepsilon_{2s\bar{\sigma}}$, $\varepsilon_{2s\sigma}$, $\varepsilon_{2p\bar{\sigma}}$, and $\varepsilon_{2p\sigma}$ of the isolated atom in the ground and excited electronic configurations discussed above. The $-(\sum_{\vec{R}_s} V_{m,m}^{Z_s,\vec{R}_s})$ term accounts for the one-electron contributions (electron-nuclei interactions); $\tilde{J}_{m,i\vec{R}_s}$ and $\tilde{J}^x_{m,i\vec{R}_s}$ are the direct and exchange Coulomb integrals calculated up to a second-order expansion in the overlap $S_{m,i\vec{R}_s}$ of the symmetric orthogonal basis set.[35] $\Delta E_{m,i\vec{R}_s}$ corresponds to the difference between the projectile atom and surface atom energy terms, and $V^{\rm dim}_{m,i\vec{R}_s}$ is the off-diagonal term that also includes the two-electron contributions to the hopping within a mean-field approximation. The super index "dim" indicates that it is calculated within the orthogonal basis set for the corresponding dimmer $(0,\vec{R}_s)$. We used the atomic basis for the C and He atoms provided in Ref. 36. The $2s$ and $2p$ Gaussian orbitals used for the He atom[37] well approximate the energy of the first excited state ^3S of He, 19.73 eV against the experimental one of 19.82 eV,[38] and also the energy of the excited state ^3P, 20.5 eV compared with the experimental value 20.96 eV.[38]

The effect of the long-range interactions is introduced by considering the image potential that defines the behavior for large normal distances (z) to the surface ($z > z_a$):

$$\varepsilon_m(R) = \begin{cases} \tilde{\varepsilon}_m(R) + V_I(z_a) & \text{for} \quad z \leqslant z_a \\ \varepsilon_m(R) + V_I(z) & \text{for} \quad z > z_a, \end{cases} \quad (4)$$

where

$$V_I(z) = \frac{1}{4(z - z_I)},$$

with $z_I = 3.16$ a.u. (defined as $d/2$, with d the interplanar distance) for the HOPG surface, and $z_a = 8$ a.u. was chosen to join the Hartree-Fock result $\tilde{\varepsilon}_m(R)$ with the correct behavior determined by the image potential contribution at large distances.

In Fig. 1(a), we show the variation with the distance to the surface of the one-electron energy levels associated with the different neutralization channels and referred to the Fermi energy of HOPG; the local density of states of HOPG[39,40] is also included in the figure. In this case we considered the interaction of the He atom with the scatter C atom and its first neighbors (see inset in Fig. 1), while in panel (b) of Fig. 1 the energy level variation by including the interaction with only the scatter C atom is shown. The energy levels have been rigidly shifted in order to have asymptotically the values of those for the isolated He atom.[38]

After the upward shift caused by the image potential at large distances, the effect of the short-range interactions with many C atoms, close to the surface, is to diminish the energy of the levels associated with the neutralization to excited states, locating them below the Fermi level. This fact makes possible the formation of excited neutral atoms at distances close to the surface whose survival probability will depend mainly on the projectile velocity. Moreover, the small density of states around the Fermi level of the HOPG allows us to infer a suppressed electron loss at low exit velocities of the He projectile. The more localized nature of the He-1s state makes its energy level practically insensitive to the interaction with many substrate atoms, as can be observed from Fig. 1.

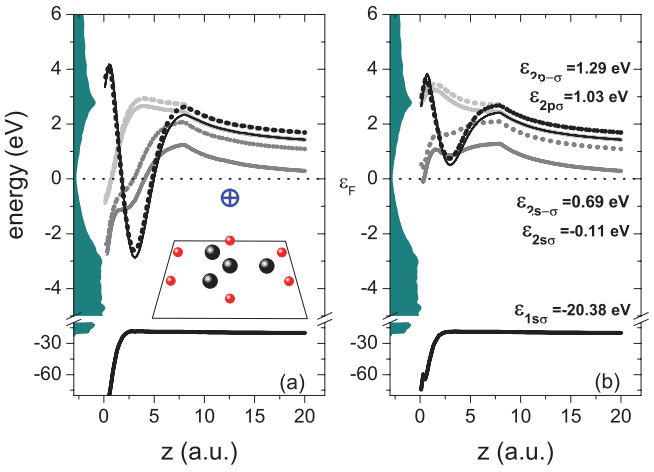

FIG. 1. (Color online) (a) The one-electron energy levels as a function of the distance to the surface by considering the interaction with the C atom beneath the He and its first neighbors (see inset): ε_{1s} (solid black line); $\varepsilon_{2s\sigma}$ (solid dark gray line); $\varepsilon_{2s\bar{\sigma}}$ (dotted dark gray line); $\varepsilon_{2p_z\sigma}$ (solid black line); $\varepsilon_{2p_z\bar{\sigma}}$ (dotted black line); $\varepsilon_{2p_{x/y}\sigma}$ (solid light gray line); and $\varepsilon_{2p_{x/y}\bar{\sigma}}$ (dotted light gray line). (b) The same but considering the interaction with only the C beneath. In panel (b) the asymptotic energy values with respect to Fermi energy ($\varepsilon_F = 0$) are indicated. The shadowed region corresponds to the local density of states of HOPG.

Therefore, by taking into account the results shown in Fig. 1, we choose the following electronic configurations: $(1s^2)$, $(1s2s)$, and $(1s2p_z)$. The neglected excited states involving the $2p_x$ and $2p_y$ orbitals are expected to have a comparatively smaller probability of occurrence according to the larger energy of the associated active level.

B. Model calculation

The following notation is defined in order to write the Hamiltonian equation (1) projected over the space of selected configurations ($\alpha = s, p$):

$$\begin{aligned} \text{He}^+(1s) &\rightarrow |1s\sigma\rangle, \\ \text{He}^+(1s^2) &\rightarrow |1s\uparrow 1s\downarrow\rangle, \\ \text{He}^*(1s\sigma 2\alpha\sigma) &\rightarrow |1s\sigma 2\alpha\sigma\rangle, \\ \text{He}^*(1s\sigma 2\alpha\bar{\sigma}) &\rightarrow |1s\sigma 2\alpha\bar{\sigma}\rangle. \end{aligned} \quad (5)$$

By projecting the Hamiltonian equation (2), we have

$$\begin{aligned} \hat{H}_{\rm atom} = {} & E(1s\uparrow)\sum_\sigma |1s\sigma\rangle\langle 1s\sigma| \\ & + E(1s\uparrow 1s\downarrow)|1s\uparrow 1s\downarrow\rangle\langle 1s\uparrow 1s\downarrow| \\ & + \sum_{\sigma,\alpha=s,p} E(1s\uparrow 2\alpha\uparrow)|1s\sigma 2\alpha\sigma\rangle\langle 1s\sigma 2\alpha\sigma| \\ & + \sum_{\sigma,\alpha=s,p} E(1s\uparrow 2\alpha\downarrow)|1s\sigma 2\alpha\bar{\sigma}\rangle\langle 1s\sigma 2\alpha\bar{\sigma}|. \end{aligned} \quad (6)$$

The interaction Hamiltonian written in the projection operator language takes the form

$$\begin{aligned}\hat{H}_{\rm int} = &\sum_{\vec{k}}[\tilde{V}_{\vec{k}1s}\hat{c}^{\dagger}_{\vec{k}\uparrow}|1s\downarrow\rangle\langle 1s\uparrow 1s\downarrow| + \text{H.c.}]\\ &- \sum_{\vec{k}}[\tilde{V}_{\vec{k}1s}\hat{c}^{\dagger}_{\vec{k}\downarrow}|1s\uparrow\rangle\langle 1s\uparrow 1s\downarrow| + \text{H.c.}]\\ &- \sum_{\vec{k},\sigma,\alpha=s,p}[\hat{V}_{\vec{k}2\alpha}\hat{c}^{\dagger}_{\vec{k}\sigma}|1s\sigma\rangle\langle 1s\sigma 2\alpha\sigma| + \text{H.c.}]\\ &- \sum_{\vec{k},\sigma,\alpha=s,p}[\hat{V}_{\vec{k}2\alpha}\hat{c}^{\dagger}_{\vec{k}\bar{\sigma}}|1s\sigma\rangle\langle 1s\sigma 2\alpha\bar{\sigma}| + \text{H.c.}], \qquad (7)\end{aligned}$$

where $\tilde{V}_{\vec{k}1s} = V_{\vec{k}1s}/\sqrt{N}$ and N accounts for the spin degeneration that in this case is 2. The Hamiltonian equation (7) provides the correct treatment of the interaction of the ground and excited states of the atom with the surface band states including the spin component; the first two terms account for the spin statistic in the ground state of the He atom. This is clearly an improvement of the rough and not justified approximation performed in Ref. 26 which includes only two states: the ground state and the excited one, assimilated to different spin components.

The quantities of interest are the probabilities of occurrence of the different He atom configurations which are defined as follows.

(1) Probability of ionization:

$$n_{\rm He^+} = \sum_{\sigma}\langle|1s\sigma\rangle\langle 1s\sigma|\rangle.$$

(2) Probability of neutralization to the ground state:

$$n_{{\rm He}^0(1s^2)} = \langle|1s\uparrow 1s\downarrow\rangle\langle 1s\uparrow 1s\downarrow|\rangle.$$

(3) Probability of neutralization to the excited $(1s2\alpha)$ state with $S_z = 1, -1$:

$$n_{{\rm He}^0(1s2\alpha,1)} = \sum_{\sigma}\langle|1s\sigma 2\alpha\sigma\rangle\langle 1s\sigma 2\alpha\sigma|\rangle.$$

(4) Probability of neutralization to the excited $(1s2\alpha)$ state with $S_z = 0$:

$$n_{{\rm He}^0(1s2\alpha,0)} = \sum_{\sigma}\langle|1s\sigma 2\alpha\bar{\sigma}\rangle\langle 1s\sigma 2\alpha\bar{\sigma}|\rangle.$$

The time evolution of the average occupation of each atom configuration is calculated by using the equation of motion in the Heisenberg picture (atomic units are used), $d\langle\hat{n}\rangle/dt = -i\langle[\hat{n},\hat{H}]\rangle$. By taking into account the energy degeneration and the normalization of the selected subspace,

$$n_{{\rm He}^+(1s)} + n_{{\rm He}^0(1s^2)} + \sum_{\alpha=s,p}[n_{{\rm He}^0(1s2\alpha,1)} + n_{{\rm He}^0(1s2\alpha,0)}] = 1,$$

we need to calculate, for instance, only the time evolutions of $\langle|1s\uparrow 1s\downarrow\rangle\langle 1s\uparrow 1s\downarrow|\rangle$, $\langle|1s\uparrow 2\alpha\uparrow\rangle\langle 1s\uparrow 2\alpha\uparrow|\rangle$, and $\langle|1s\uparrow 2\alpha\downarrow\rangle\langle 1s\uparrow 2\alpha\downarrow|\rangle$. We arrived at the following expressions by using the Hamiltonian equation (1) with Eqs. (6) and (7), for the $\hat{H}_{\rm atom}$ and $\hat{H}_{\rm int}$, respectively:

$$\begin{aligned}\frac{d\langle|1s\uparrow 1s\downarrow\rangle\langle 1s\uparrow 1s\downarrow|\rangle}{dt} &= 4\,\mathrm{Im}\sum_{\vec{k}}\tilde{V}^{*}_{\vec{k}1s}\langle|1s\uparrow 1s\downarrow\rangle\langle 1s\downarrow|\hat{c}_{\vec{k}\uparrow}|\rangle,\\ \frac{d\langle|1s\uparrow 2\alpha\uparrow\rangle\langle 1s\uparrow 2\alpha\uparrow|\rangle}{dt} &= -2\,\mathrm{Im}\sum_{\vec{k}}\hat{V}^{*}_{\vec{k}2\alpha}\langle|1s\uparrow 2\alpha\uparrow\rangle\langle\uparrow 0|\hat{c}_{\vec{k}\uparrow}|\rangle,\\ \frac{d\langle|1s\uparrow 2\alpha\downarrow\rangle\langle 1s\uparrow 2\alpha\downarrow|\rangle}{dt} &= -2\,\mathrm{Im}\sum_{\vec{k}}\hat{V}^{*}_{\vec{k}2\alpha}\langle|1s\uparrow 2\alpha\uparrow\rangle\langle\uparrow 0|\hat{c}_{\vec{k}\uparrow}|\rangle.\end{aligned}$$

The crossed terms $\langle|A\rangle\langle B|\hat{c}_{\vec{k}\sigma}|\rangle$ are obtained from the Green functions:

$$F_{|A\rangle\langle B|}(\hat{c}_{\vec{k}\sigma}) = i\langle[|A\rangle\langle B(t');\hat{c}_{\vec{k}\sigma}(t)]|\rangle$$

at equal time values $t = t'$;

$$\langle|A\rangle\langle B|c_{\vec{k}\sigma}|\rangle = (1/2)i\,F_{|A\rangle\langle B|}(\hat{c}_{\vec{k}\sigma})_{t=t'}.$$

The Green functions $F_{|A\rangle\langle B|}(\hat{c}_{\vec{k}\sigma})$ are calculated by using the equation of motion (EOM) method closed by using a second order in the hopping term criterion. The final expression is

$$\begin{aligned}F_{|A\rangle\langle B|}(\hat{c}_{\vec{k}\sigma})_{t=t'} = -i\int_{t_0}^{t}d\tau\,V_{\vec{k}\beta}[&F_{|A\rangle\langle B|}(\tau,t)\\ &-(2\langle\hat{n}_{\vec{k}\sigma}\rangle - 1)G_{|A\rangle\langle B|}(\tau,t)]e^{i\varepsilon_{\vec{k}}(\tau-t)}. \qquad (8)\end{aligned}$$

The Green functions $F_{|A\rangle\langle B|}(\tau,t)$ and $G_{|A\rangle\langle B|}(\tau,t)$ in Eq. (8) are given by

$$\begin{aligned}G_{|A\rangle\langle B|}(\tau,t) &= i\Theta(t-\tau)\langle|\{|A\rangle\langle B|(t);|B\rangle\langle A|(\tau)\}|\rangle,\\ F_{|A\rangle\langle B|}(\tau,t) &= i\langle|[|A\rangle\langle B|(t);|B\rangle\langle A|(\tau)]|\rangle,\end{aligned} \qquad (9)$$

where $[;]$ and $\{;\}$ indicate commutator and anticommutator, respectively. These Green functions are also calculated by the EOM method up to a second order in the hopping terms.

C. Time evolution of Green functions $G_{|A\rangle\langle B|}(t,t')$ and $F_{|A\rangle\langle B|}(t,t')$

The equations of motion of the Green functions, Eqs. (9), start with the expressions

$$\begin{aligned}i\frac{G_{|A\rangle\langle B|}(t,t')}{dt} &= \delta(t-t')\langle|\{|A\rangle\langle B|(t');|B\rangle\langle A|(t')\}|\rangle\\ &\quad + i\Theta(t'-t)\langle|\{|A\rangle\langle B|(t');[|B\rangle\langle A|;\hat{H}]_t\}|\rangle\\ i\frac{F_{|A\rangle\langle B|}(t,t')}{dt} &= i\langle|[|A\rangle\langle B|(t');[|B\rangle\langle A|;\hat{H}]_t]|\rangle.\end{aligned}$$

The next step in the particular case of $G_{|A\rangle\langle B|}(t,t')$ with $A = 1s\uparrow 1s\downarrow$ and $B = 1s\uparrow$ leads to the expression

$$\begin{aligned}i\frac{d}{dt}&G_{|A\rangle\langle B|}(t,t')\\ &= \varepsilon_{1s}G_{|A\rangle\langle B|}(t,t') + \delta(t-t')\langle|1s\uparrow 1s\downarrow\rangle\langle 1s\uparrow 1s\downarrow|\\ &\quad + |1s\uparrow\rangle\langle 1s\uparrow|\rangle + \sum_{\vec{k}\sigma}\mathrm{sgn}(\sigma)\tilde{V}^{*}_{\vec{k}1s}G_{|A\rangle\langle B|}(|1s\uparrow\rangle\langle 1s\bar{\sigma}|\hat{c}_{\vec{k}\sigma})\\ &\quad - \sum_{\vec{k}}\tilde{V}^{*}_{\vec{k}1s}G_{|A\rangle\langle B|}(|1s\uparrow\rangle\langle 1s\downarrow|\hat{c}_{\vec{k}\downarrow})\\ &\quad - \sum_{\vec{k},\sigma,\alpha=s,p}\hat{V}^{*}_{\vec{k}2\alpha}G_{|A\rangle\langle B|}(|1s\uparrow 2\alpha\sigma\rangle\langle 1s\uparrow 1s\downarrow|\hat{c}_{\vec{k}\sigma}). \qquad (10)\end{aligned}$$

We now have to calculate the new Green functions appearing in Eq. (10); for instance, the motion equation of $G_{|A\rangle\langle B|}(|1s\uparrow 2\alpha\sigma\rangle\langle 1s\uparrow 1s\downarrow|\hat{c}_{\vec{k}\sigma})$ is

$$\begin{aligned} i\frac{d}{dt}&G_{|A\rangle\langle B|}(|1s\uparrow 2\alpha\sigma\rangle\langle 1s\uparrow 1s\downarrow|\hat{c}_{\vec{k}\sigma}) \\ &= -\delta(t-t')\langle|1s\uparrow 1s\uparrow 2\alpha\sigma\rangle\langle 1s\uparrow 1s\uparrow|\hat{c}_{\vec{k}\sigma}\rangle \\ &\quad + (\varepsilon_{\vec{k}} + \varepsilon_{1s} - \varepsilon_{2\alpha\sigma})G_{|A\rangle\langle B|}(|1s\uparrow 2\alpha\sigma\rangle\langle 1s\uparrow 1s\downarrow|\hat{c}_{\vec{k}\sigma}) \\ &\quad - \sum_{\vec{K}} \hat{V}^{*}_{\vec{K}2\alpha} G_{|A\rangle\langle B|}(|1s\uparrow\rangle\langle 1s\uparrow 1s\downarrow|\hat{c}^{\dagger}_{\vec{K}\sigma}\hat{c}_{\vec{k}\sigma}). \end{aligned} \tag{11}$$

From Eqs. (10) and (11) one can infer the following sequence of electron transitions:

$$|1s\uparrow\rangle \rightarrow \hat{V}_{\vec{K}2\alpha\sigma}\hat{c}_{\vec{K}\sigma} \rightarrow |1s\uparrow 2\alpha\sigma\rangle \rightarrow \hat{V}^{*}_{\vec{k}2\alpha\sigma}\hat{c}^{\dagger}_{\vec{k}\sigma} \rightarrow |1s\uparrow\rangle;$$

beginning from the ionic state an electron is destroyed in the band and created in the $(2\alpha\sigma)$ atomic orbital, then an electron is destroyed in this atomic orbital and transferred to a band state, coming back in this form to the ionic configuration.

A closure criterion based on second-order approximation in the coupling $\hat{V}_{\vec{k}\sigma}$ is used and mean-field approximations like the following are performed:

$$G_{|A\rangle\langle B|}(|1s\uparrow\rangle\langle 1s\uparrow 1s\downarrow|\hat{c}^{\dagger}_{\vec{K}\sigma}\hat{c}_{\vec{k}\sigma}) = \langle\hat{c}^{\dagger}_{\vec{K}\sigma}\hat{c}_{\vec{k}\sigma}\rangle\delta_{\vec{k}\vec{K}}G_{|A\rangle\langle B|}(t,t').$$

By considering the phase transformation

$$\begin{aligned} &G(F)_{|A\rangle\langle B|}(t,t') \\ &\quad = \exp\left\{-i\int_{t'}^{t}[E(|A\rangle) - E(|B\rangle)]d\tau\right\} g(f)_{|A\rangle\langle B|}(t,t'), \end{aligned}$$

we finally arrived at the expressions

$$\begin{aligned} i\frac{d}{dt}&g_{|A\rangle\langle B|}(t,t') \\ &= \delta(t-t')\langle|[|1s\uparrow 1s\downarrow\rangle\langle 1s\uparrow 1s\downarrow| + |1s\uparrow\rangle\langle 1s\uparrow|]|\rangle + i\sum_{\vec{k}}\left[\tilde{V}^{*}_{\vec{k}1s}(t)\langle|1s\uparrow 1s\downarrow\rangle\langle 1s\downarrow|\hat{c}_{\vec{k}\uparrow}\rangle_{t'}\exp\left(i\int_{t'}^{t}\varepsilon_{1s}\,dx\right)\right. \\ &\quad \left. + \sum_{\sigma,\alpha=s,p}\hat{V}^{*}_{\vec{k}2\alpha}(t)\langle|1s\uparrow 2\alpha\sigma\rangle\langle 1s\uparrow|\hat{c}_{\vec{k}\sigma}\rangle_{t'}\exp\left(i\int_{t'}^{t}\varepsilon_{2\alpha\sigma}dx\right)\right]e^{-i\varepsilon_{\vec{k}}(t-t')} \\ &\quad + \int_{-\infty}^{\infty}d\tau\left\{\left[\Xi^{0}_{1s}(t,\tau) + \Xi^{>}_{1s,\uparrow}(t,\tau)\right]\exp\left(-i\int_{t}^{\tau}\varepsilon_{1s}\,dx\right) + \sum_{\sigma,\alpha=s,p}\Xi^{<}_{2\alpha,\sigma}(t,\tau)\exp\left(-i\int_{t}^{\tau}\varepsilon_{2\alpha\sigma}\,dx\right)\right\} g_{|A\rangle\langle B|}(\tau,t') \end{aligned} \tag{12}$$

$$\begin{aligned} i\frac{d}{dt}&f_{|A\rangle\langle B|}(t,t') \\ &= i\sum_{\vec{k}}\left[\langle 2\hat{n}_{\vec{k}\uparrow} - 1\rangle\tilde{V}^{*}_{\vec{k}1s}(t)\langle|1s\uparrow 1s\downarrow\rangle\langle 1s\downarrow|\hat{c}_{\vec{k}\uparrow}\rangle_{t'}\exp\left(i\int_{t'}^{t}\varepsilon_{1s}\,dx\right)\right. \\ &\quad \left. + \sum_{\sigma,\alpha=s,p}\langle 2\hat{n}_{\vec{k}\sigma} - 1\rangle\hat{V}^{*}_{\vec{k}2\alpha}(t)\langle|1s\uparrow 2\alpha\sigma\rangle\langle 1s\uparrow|\hat{c}_{\vec{k}\sigma}\rangle_{t'}\exp\left(i\int_{t'}^{t}\varepsilon_{2\alpha\sigma}\,dx\right)\right]e^{-i\varepsilon_{\vec{k}}(t-t')} \\ &\quad + \int_{-\infty}^{\infty}d\tau\left\{\left[\Xi^{0,R}_{1s}(t,\tau) + \Xi^{>,R}_{1s,\uparrow}(t,\tau)\right]\exp\left(-i\int_{t}^{\tau}\varepsilon_{1s}\,dx\right) + \sum_{\sigma,\alpha=s,p}\Xi^{<,R}_{2\alpha,\sigma}(t,\tau)\exp\left(-i\int_{t}^{\tau}\varepsilon_{2\alpha\sigma}\,dx\right)\right\} f_{|A\rangle\langle B|}(\tau,t') \\ &\quad + \int_{-\infty}^{\infty}d\tau\left\{\left[\Omega^{0}_{1s}(t,\tau) + \Omega^{>}_{1s,\uparrow}(t,\tau)\right]\exp\left(-i\int_{t}^{\tau}\varepsilon_{1s}\,dx\right) + \sum_{\sigma,\alpha=s,p}\Omega^{<}_{2\alpha,\sigma}(t,\tau)\exp\left(-i\int_{t}^{\tau}\varepsilon_{2\alpha\sigma}\,dx\right)\right\} g_{|A\rangle\langle B|}(\tau,t'). \end{aligned} \tag{13}$$

In Eqs. (12) and (13) $\langle n_{\vec{k}\sigma}\rangle$ is given by the Fermi function at a temperature T. The case $A = 1s\uparrow 2\alpha\sigma$ and $B = 1s\uparrow$, and the expressions of the self-energies are presented in Appendix.

D. LCAO expansion of the solid band states: Atom-atom couplings and density matrix of the solid

The LCAO expansion of the $\phi_{\vec{k}}$ states allows writing

$$\hat{V}_{\vec{k}\beta}(\vec{R}) = \sum_{i,\vec{R}_s} c^{\vec{k}}_{i,\vec{R}_s}\langle\phi_i(\vec{r}-\vec{R}_s)|\hat{V}|\phi_\beta(\vec{r}-\vec{R})\rangle, \tag{14}$$

which is a superposition of the atom-atom couplings ($\vec{R}$ is the projectile atom position with respect to the scatter surface atom) weighted by the coefficients $c^{\vec{k}}_{i,\vec{R}_s}$ that define the density matrix of the solid, $\rho_{i\vec{R}_s,j\vec{R}_{s'}}$. In this form, the localized nature of the atoms and the extended features of the surface enter in the calculation of the charge exchange between ions and surfaces. The Anderson hybridization width associated with each atomic orbital,

$$\Gamma_\beta(\varepsilon,\vec{R}) = \pi\sum_{\vec{k}}|\hat{V}_{\vec{k}\beta}(\vec{R})|^2\delta(\varepsilon - \varepsilon_{\vec{k}}),$$

is calculated as

$$\Gamma_\beta(\varepsilon,\vec{R}) = \pi \sum_{i\vec{R}_s, j\vec{R}_{s'}} V^*_{\beta i,\vec{R}_s}(\vec{R}) V_{\beta j,\vec{R}_{s'}}(\vec{R}) \rho_{i\vec{R}_s, j\vec{R}_{s'}}(\varepsilon). \quad (15)$$

The self-energies [Eqs. (A3)–(A8)] and terms like $\sum_{\vec{k}} \hat{V}^*_{\vec{k}2\alpha} \langle |A\rangle\langle B| \hat{c}_{\vec{k}\sigma}\rangle$ are calculated in analogous form by considering the LCAO expansion of the band states of the solid.

III. RESULTS AND DISCUSSION

The He atom is moving perpendicular to the surface with a constant velocity $v_{\text{in(out)}} = v * \sin(\theta_{\text{in(out)}})$, along a trajectory described by $z_{\text{in(out)}} = z_{rtp} + v_{\text{in(out)}}|t|$, with z_{rtp} the distance of closest approach to the surface, v the incoming ion velocity, and $\theta_{\text{in(out)}}$ the angle between the trajectory direction and the surface. The values of z_{rtp} are obtained from the He-C interaction potential: $z_{rtp} = 0.24$ a.u. is considered for incoming energies between 1 and 1.5 keV and $z_{rtp} = 0.14$ a.u. for energy values larger than 1.5 keV. The kinetic energy loss of helium ions in the elastic scattering by C atoms is taken into account, $E_{\text{out}} = 0.305 E_{\text{in}}$, with $E_{\text{in(out)}}$ the incoming(exit) kinetic energy of the projectile ion. The value 0.305 corresponds to the classical binary He-C collision for the experimental geometry (*scattering angle* =135°). We consider $\theta_{\text{in}} = 45°$ and $\theta_{\text{out}} = 90°$ according to the experimental geometry of Ref. 26.

The atomic hopping integrals $V_{\beta j,\vec{R}_{s'}}(\vec{R})$ are shown in Fig. 2 for helium orbitals $\beta = 1s$, $2s$, and $2p_z$ and the states $j = 2s$ and $2p_z$ of the C scatter atom.

We observe from Fig. 2 that the couplings between the He-1s and the C-2s and C-2p states are stronger than the corresponding couplings of the $2s$ and $2p_z$ states of He at distances close to the surface. For z values larger than 4 a.u. the atomic hopping integrals involving He excited states become more significant and show a marked extended behavior. We found that in the case of He-1s, the couplings with the orbital states of the nearest C atom (the central one in the inset of Fig. 1) are practically determining the LCAO expansion equation (14), while in the He-2s and He-2p cases, it is necessary to also include the three C atoms nearest to the central one.

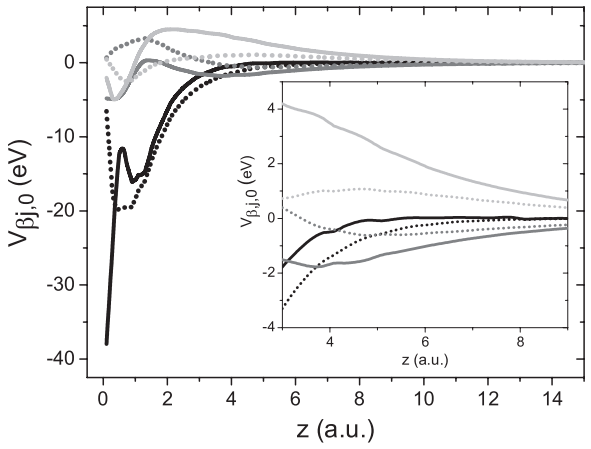

FIG. 2. Atomic coupling terms $V_{\beta j,\vec{R}_{s'}}$ between He and the scatter C atom ($\vec{R}_s = 0$); β indicating the He orbitals: 1s (black line), 2s (dark gray line), and $2p_z$ (light gray line); j indicating the C orbitals: 2s (solid lines) and $2p_z$ (dotted lines). The inset is a blow up of the large distance region.

A. The ground state of the He atom as the unique neutralization channel

1. Spinless approximation

The simplest approximation in this case is to ignore the spin in the Anderson Hamiltonian: There is only one active spinless electron involved in the charge fluctuation $He^+(1s^0) \leftrightarrow He^0(1s^1)$.[41] In Fig. 3 we show the neutral fraction calculated in this way as a function of the incoming ion energy. In this figure we compare the results obtained by considering the interaction with only the scatter C atom with those obtained by including the interaction with the first neighbors too.

We can see that for incoming energies $E_{\text{in}} > 1$ keV the neutral fraction predicted by this simple approximation to the collision process is between 40% and 50% in the case of considering the interaction with the four nearest C atoms, while it varies between 30% and 40% in the case of He interacting only with the C beneath. A slight oscillatory behavior is observed in both cases in this energy range. The adiabatic picture based on the level shift and its width provides a first attempt to understand the behavior of the neutral fraction with the incoming energy. The level width calculated as $\Gamma_{1s}(\varepsilon_{1s},z)$ [Eq. (15)] is shown in Fig. 4. From this figure we can see that the inclusion of the nearest neighbors in the expansion LCAO [Eq. (14)] leads to an increase of the He-1s level width for distances close to the surface, thus explaining the larger neutral fraction observed in Fig. 3.

The oscillatory behavior of the neutral fraction with projectile energy (velocity) depends strongly on the z dependence of the ion energy level (Fig. 4) and of the atomic hopping terms (Fig. 2), as can be seen in Fig. 5. Figure 5 shows a comparison with neutral fractions calculated by (i) assuming that the energy level remains constant for distances $z < 3$ a.u.

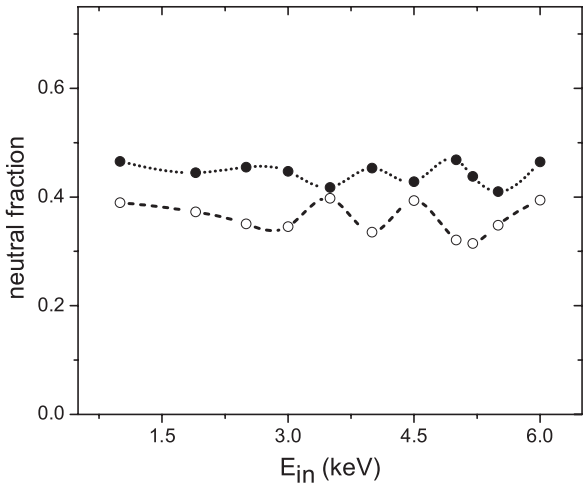

FIG. 3. Neutral fraction as a function of the incoming ion energy calculated by considering only the He ground state and within the spinless approximation. Including only the scatter C atom (empty circles), and the four nearest C atoms (full circles) in the LCAO expansion equation (14).

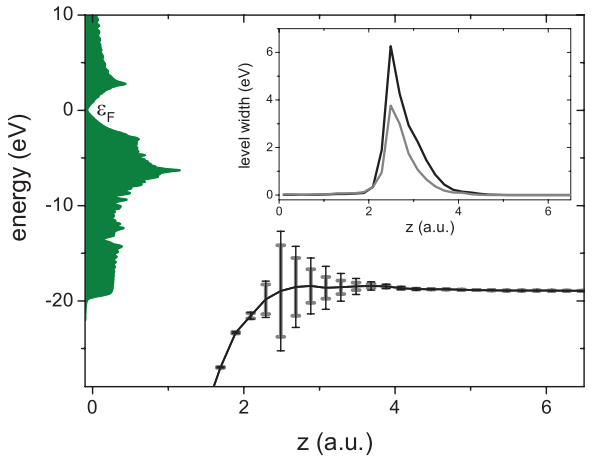

FIG. 4. (Color online) The ionization level (solid line) as a function of the distance to the surface and the widths calculated by Eq. (15) shown as error bars: including only the scatter C atom (gray bars) and the four nearest C atoms (black bars) in the LCAO expansion [Eq. (14)]. In the inset the same level widths are shown as a function of the distance to the surface.

and (ii) assuming a constant turning point given by $z_{rtp} = 1.3$ a.u. in order to have a smoother variation of the hopping terms along the ion trajectory. The differences are more pronounced for E_{in} larger than 4 keV, that is, for these energy values the neutral fraction is determined at distances smaller than 3 a.u. where the three calculations differ effectively. We observe in the evolution of the neutral fraction along the trajectory (see the inset in Fig. 5) that not only an electron capture process is occurring but also an electron loss in the region close to the surface due to the large coupling between

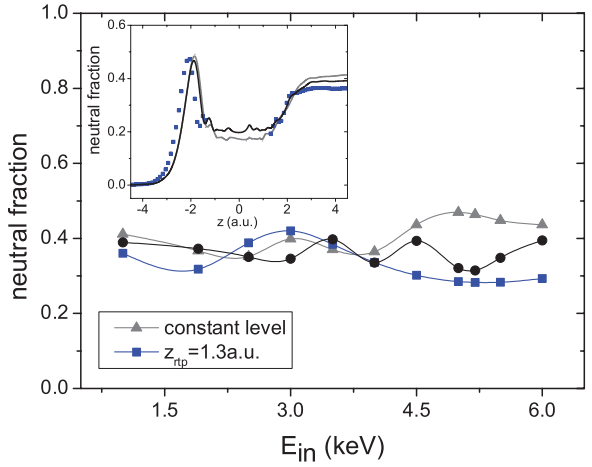

FIG. 5. (Color online) The neutral fraction as a function of the ion incoming energy within the spinless approximation by considering only the interaction with the scatter C atom: (i) calculation of Fig. 3 (solid circles); (ii) by maintaining constant the ionization level for distances smaller than 3 a.u. (solid up triangles); and (iii) by considering the turning point equal to $z_{rtp} = 1.3$ a.u (solid squares). The inset shows the neutral fraction as a function of the ion trajectory ($z < 0$ corresponds to the incoming trajectory and $z > 0$ to the outgoing path) at $E_{\text{in}} = 1$ keV for the same cases: (i) solid black line, (ii) gray solid line, and (iii) square symbols.

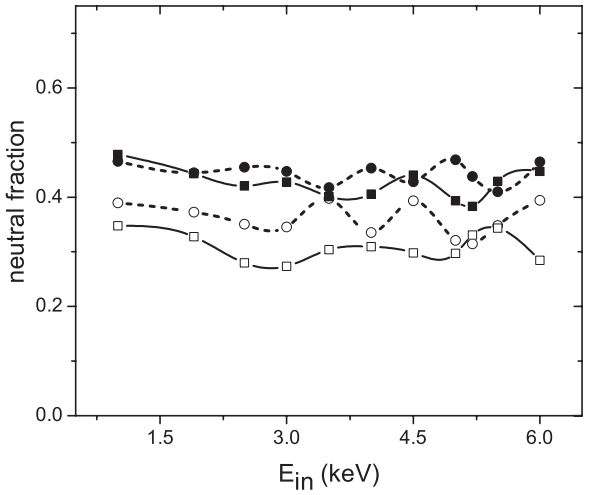

FIG. 6. The neutral fraction as a function of the incoming ion energy by considering only the ground state: the calculation that includes spin statistic effects (squares) and the spinless calculation (circles). Empty symbols correspond to the interaction with only the scatter C atom, while full symbols correspond to the calculation including the interaction with the four nearest C atoms.

the He-1s and the C states that allows for promoting the electron to empty band states.

2. *By including the spin statistics*

An interesting improvement to the spinless calculation is to consider the spin fluctuation statistic that is equivalent to an infinite correlation limit approximation of the Anderson Hamiltonian.[30,42–45] This means, in our proposal, to consider $\text{He}^0(1s^2) \leftrightarrow \text{He}^+(1s)$ transition, disregarding the possibility of a double ionized charge configuration (He^{++}). In Fig. 6 we can see that the neutral fraction does not change appreciably by including the spin statistic effects through the new contributions to the dynamical level shift and width provided by the self-energy $\Xi^{>}_{1s\sigma}$ [Eq. (A5)]. Nevertheless, the differences introduced by considering the interaction of He with the nearest C atoms are more pronounced in this case.

B. The excited states as possible neutralization channels

1. *By including the He(1s2s) excited configuration*

The results shown in Fig. 7(a) were obtained by considering the He($1s2s$) excited configuration and the interaction with only the C scatter atom, while in Fig. 7(b) the interaction of the He atom with the nearest carbon atoms of the HOPG surface was taken into account.

We can observe marked differences between considering one and four C atoms in the He-surface interaction. In Fig. 7(a), the contribution of the ground state to the ion neutralization, between 40% and 50%, has increased compared with the values between 30% and 40% in the case in which the ground state is only one neutralization channel (see Fig. 6). However, in both cases the slight oscillatory behavior with the incoming energy is similar. The contribution of the excited configuration ($1s2s$) to the ion neutralization varies between 35% and 10%, showing a decaying behavior as the incoming energy decreases. We can

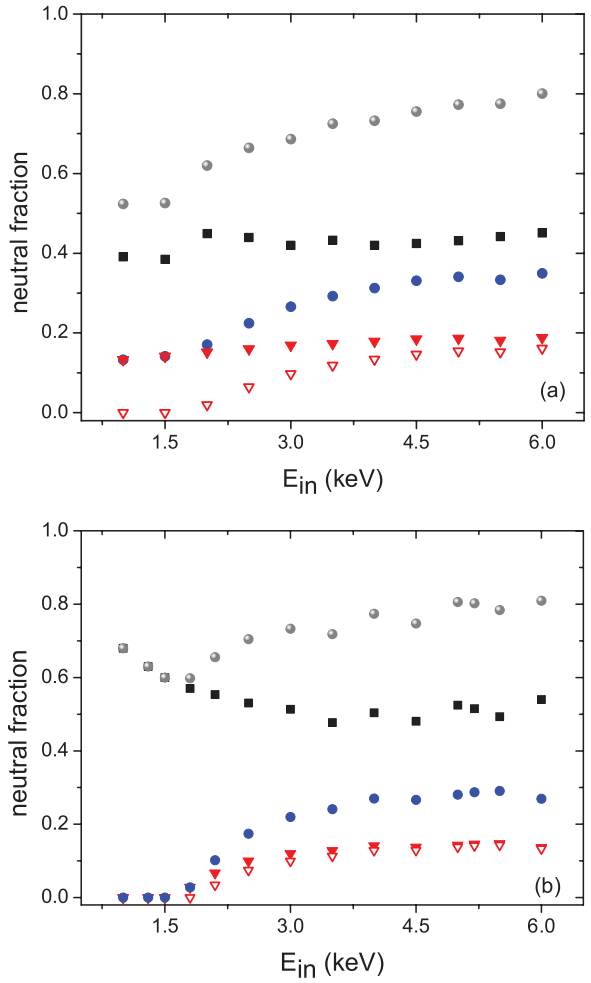

FIG. 7. (Color online) The neutral fraction as a function of the incoming ion energy: $(1s2s)$ with $S_z = 1, -1$ contribution (solid down triangles), $(1s2s)$ with $S_z = 0$ contribution (open down triangles), $(1s^2)$ contribution (solid squares), total contribution from excited states (solid circles), and the total neutral fraction (gray spheres). (a) The interaction with only the C beneath is considered; (b) the four nearest C atoms are taken into account.

see from Fig. 7(a) that this decaying with energy behavior is mainly determined by the probability of neutralization to the excited $(1s2s)$ configuration with $S_z = 0$. Thus, the total neutral fraction $n_{\mathrm{He}^0(1s^2)} + n_{\mathrm{He}^0(1s2s,1)} + n_{\mathrm{He}^0(1s2s,0)}$ decays as energy decreases, varying from 80% to 50%.

In the case of considering the interaction with the nearest C atoms of the surface [Fig. 7(b)], the probability of neutralization to the ground state $n_{\mathrm{He}^0(1s\sigma)}$ oscillates slightly at high energy values around 50% and increases at lower energies ($E_{\mathrm{in}} < 3$ keV) arriving at a contribution of 70% at 1 keV. The total probability of neutralization to the excited states is nearly constant (between 20% and 30%) for $E_{\mathrm{in}} > 3$ keV, and diminishes to zero for incoming energies below 1.5 keV. Both excited states, with $S_z = 0$ and 1, show contributions with similar energy dependence.

2. *By including the He(1s2s) and He(1s2p) excited configurations*

The different contributions to the ion neutralization in the case of also including the excited configuration $(1s2p)$ as a possible neutralization channel are shown in Fig. 8. In part (a) of this figure the results were obtained by considering the interaction with only the C scatter atom, while in part (b) the calculation includes the four nearest C atoms of the HOPG surface.

The contribution of the ground state to the neutralization increases when the interaction with the nearest C atoms is taken into account, nevertheless the energy dependence practically does not change. This is not the case for the excited states contribution; in the case of considering only the interaction with the scatter C atom, the neutralization to the $(1s2p)$ is negligible and the total contribution of the excited $(1s2s)$ configuration is nearly constant with the incoming energy and larger than in the case of considering the four nearest C atoms in the LCAO expansion [Eq. (14)]. We can observe from Fig. 8 that the contribution of the ground state shows an overall increase compared with the case of considering only the excited $(1s2s)$ configuration (see Fig. 7).

In Fig. 8(b), we can see that the ground state contribution is between 60% and 80%, the excited states contribution varies from 10% to 35%, and the total neutralization shows a slight oscillatory behavior, reaching the value of 100% for energies between 2 and 4 keV. The calculated neutral fraction at an incoming energy of 5 keV is 0.93, which is very similar to the reported value of 0.95 measured in ion backscattering experiments.[26]

A remarkable point is that nevertheless the contribution of the excited states to the neutralization decreases at low energies; a larger neutralization to the ground state occurs when excited states are included in the configuration space, as shown in Fig. 9 (here the results are obtained by taking into account the four nearest C atoms).

We can explain the results summarized in Fig. 9 by returning to the adiabatic picture based on the shift and broadening of the energy level, extracted from the hybridization function. In the spinless case, this hybridization function is simply

$$\Sigma^0_{1s}(\omega) = \sum_{\vec{k}} \frac{|\tilde{V}_{\vec{k}1s}|^2}{\omega - \varepsilon_{\vec{k}} - i\eta}.$$

By taking into account the contributions from the spin statistics and excited states, we can define the following extended hybridization function [Fourier transform of Eq. (12)]:

$$\Sigma_{1s\sigma}(\omega) = \Sigma^0_{1s}(\omega) + \sum_{\vec{k}} \frac{|\tilde{V}_{\vec{k}1s}|^2 \langle 1 - n_{\vec{k}\sigma}\rangle}{\omega - \varepsilon_{\vec{k}} - i\eta} + \sum_{\vec{k},\sigma',\alpha=s,p} \frac{|\hat{V}_{\vec{k}2\alpha}|^2 \langle n_{\vec{k}\sigma'}\rangle}{\omega - \varepsilon_{\vec{k}} + \varepsilon_{2\alpha\sigma'} - \varepsilon_{1s} - i\eta}. \quad (16)$$

In an approximated way, the real part of Eq. (16) can be identified with the energy level shift and the imaginary part with its broadening. In Fig. 10, $Re\Sigma_{1s\sigma}(\omega)$ and $Im\Sigma_{1s\sigma}(\omega)$ evaluated in $\omega = \varepsilon_{1s}$ are shown as a function of the distance to the surface.

Accordingly to the shifts of the ionization level presented in Fig. 10, the spinless calculation and that including the spin

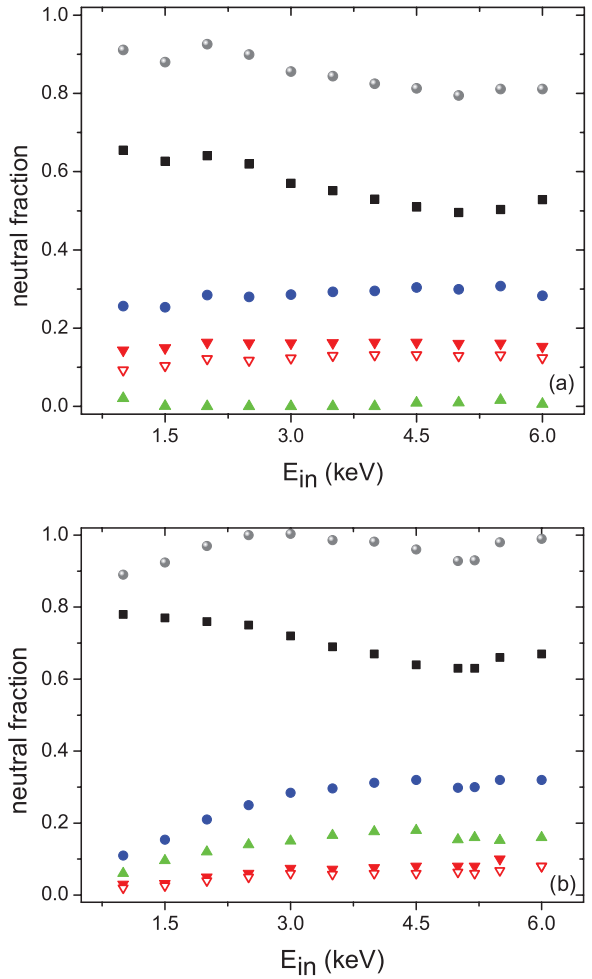

FIG. 8. (Color online) The neutral fraction as a function of the incoming ion energy: $(1s2s)$ with $S_z = 1, -1$ contribution (solid down triangles), $(1s2s)$ with $S_z = 0$ contribution (open down triangles), the total $(1s2p)$ contribution (solid up triangles), $(1s^2)$ contribution (solid squares), total contribution from excited states (solid circles), and the total neutral fraction (gray spheres). (a) The interaction with only the C beneath is considered; (b) the four nearest C atoms are taken into account.

statistic would not differ largely, being less neutralization is expected in the second case due to the smaller hybridization width. When including the excited $(1s2s)$ configuration, an increasing neutralization is expected at low incoming energies due to a pronounced upward shift of the energy level at large distances produced by the interaction between the atom excited state and the surface [third term of Eq. (16)]. The inclusion of the $(1s2p)$ excited configuration leads to a more pronounced upward shift of the ionization level and to a larger hybridization with the band states at distance values between 3 and 5 a.u. A larger probability of neutralization to the ground state is expected in the last case in all the energy ranges analyzed. In this form, we can understand the corresponding results shown in Fig. 9.

Analogously, the behavior of the contribution to the neutral fraction by the excited states shown in Figs. 7 and 8 can be explained taking into account the corresponding hybridization

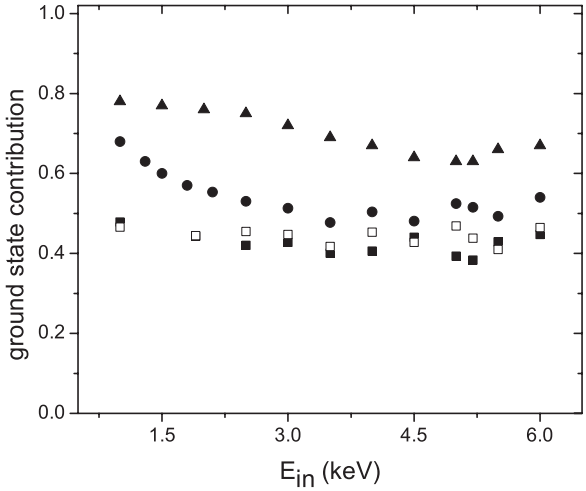

FIG. 9. The contribution of the ground state to the neutral fraction as a function of the incoming ion energy: spinless calculation (empty squares), by including spin statistic effects (full squares), by considering the excited $(1s2s)$ configuration (full circles), by considering both, the $(1s2s)$ and the $(1s2p)$ excited configurations (full up triangles).

self-energy:

$$\Sigma_{2\alpha\sigma}(\omega) = \sum_{\vec{k}} \frac{|\hat{V}_{\vec{k}2\alpha\sigma}|^2}{\omega - \varepsilon_{\vec{k}} - i\eta} + \sum_{\vec{k}} \frac{|\tilde{V}_{\vec{k}1s}|^2 \langle n_{\vec{k}\sigma}\rangle}{\omega - \varepsilon_{\vec{k}} + \varepsilon_{1s} - \varepsilon_{2\alpha\sigma} - i\eta} + \sum_{\vec{k},(\beta\sigma')\neq(\alpha\sigma)} \frac{|\hat{V}_{\vec{k}2\alpha}|^2 \langle n_{\vec{k}\sigma'}\rangle}{\omega - \varepsilon_{\vec{k}} + \varepsilon_{2\beta\sigma'} - \varepsilon_{2\alpha\sigma} - i\eta}. \quad (17)$$

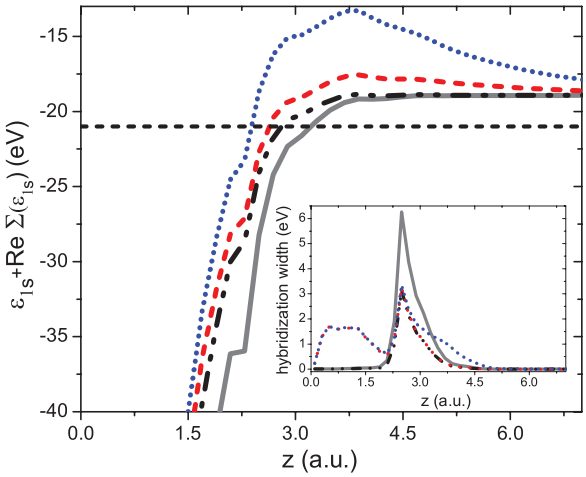

FIG. 10. (Color online) $\varepsilon_{1s} + \mathrm{Re}\,\Sigma_{1s\sigma}(\omega)$ evaluated in $\omega = \varepsilon_{1s}$ as a function of the distance to the surface (the four nearest C atoms are included): only the noninteracting self-energy (gray solid line), the self-energy that includes the spin statistic effect (dash-dot-dot line), by including the contribution to $\Sigma_{1s\sigma}(\omega)$ provided by the presence of the $(1s2s)$ excited state (dashed line), and also the contribution by the presence of the $(1s2p)$ excited state (dotted line). The horizontal dashed line indicates the bottom of the valence band. In the inset, $\mathrm{Im}\,\Sigma_{1s\sigma}(\omega)$ is shown by using the same symbols in the different cases.

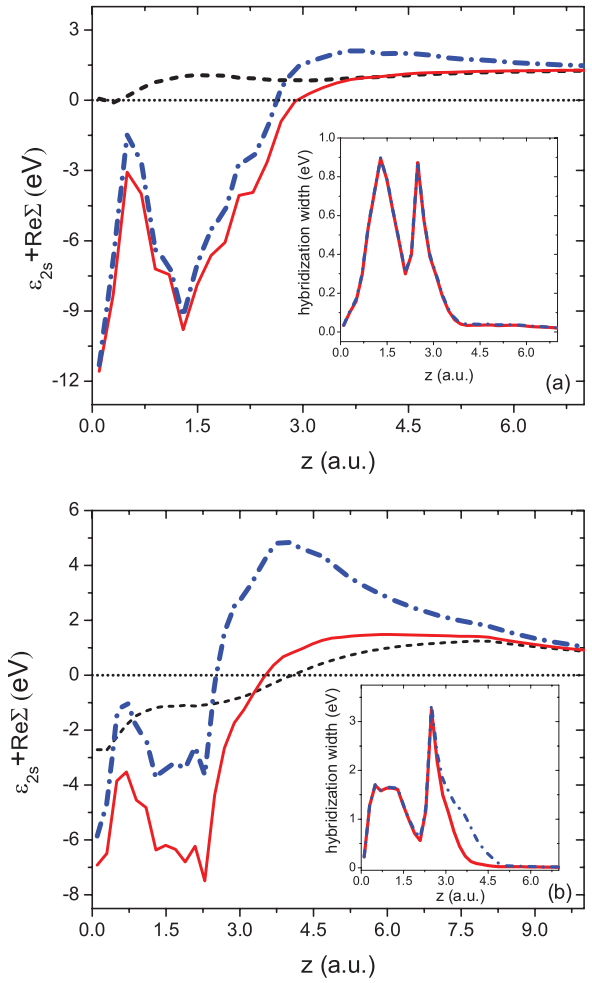

FIG. 11. (Color online) $\varepsilon_{2s\sigma} + \mathrm{Re}\,\Sigma_{2s\sigma}(\varepsilon_{2s\sigma})$ as a function of the distance to the surface: by including the contributions to $\Sigma_{2s\sigma}(\omega)$ provided by the presence of the ground state $(1s^2)$ and the $(1s2s)$ with $S_z = 0$ excited state (solid line); adding also the contribution by the presence of the $(1s2p)$ excited state (dash-dotted line). The dashed line is the energy level $\varepsilon_{2s\sigma}$. In the inset, $\mathrm{Im}\,\Sigma_{2s\sigma}(\varepsilon_{2s\sigma})$ is shown by using the same type of lines in the different cases. (a) The interaction with only the C beneath is considered; (b) the four nearest C atoms are taken into account.

Let us analyze the contribution of the $(1s2s)$ configuration with $S_z = 1, -1$. The $\mathrm{Re}\,\Sigma_{2s\sigma}(\varepsilon_{2s\sigma})$ and $\mathrm{Im}\,\Sigma_{2s\sigma}(\varepsilon_{2s\sigma})$ are shown in Fig. 11 in the case of considering the interaction with only the scatter C atom [panel (a)], and also including the nearest neighbors [panel (b)].

In the case of considering the interaction with only one C atom, the shift of the energy level below the Fermi energy due to the correlation effects explains the significant occupation of the excited configuration. In this case, the hybridization width is provided by the imaginary part of the first two terms of Eq. (17), therefore it is the same including or not the $(1s2p)$ excited configuration. The more pronounced upward shift of $\varepsilon_{2s\sigma}$ when including the presence of the excited state $(1s2p)$ leads to a larger electron loss probability and therefore to a smaller contribution of the excited $(1s2s)$ state to the neutral fraction, as can be seen from Fig. 8(a) compared with Fig. 7(a).

In the case of including the interaction with the first four C neighbors, the different contributions of the $(1s2s)$ configuration observed by considering [Fig. 8(b)] and not considering [Fig. 7(b)] the presence of the excited $(1s2p)$ state, respond quite well to the adiabatic picture described by the level shift and width [Fig. 11(b)]. A more pronounced upward shift is associated with a lesser contribution to the neutralization but a larger broadening is, on the other hand, favoring electron loss and capture processes when the energy level is around the Fermi level.

In summary, the behavior of the neutral fraction with the energy of the incoming ion is consistent with the variation along the trajectory of the shift and broadening of the involved energy levels, extracted from the extended hybridization functions, Eqs. (16) and (17).

The neutralization probability as a function of the ion trajectory evidences the more complex features of the time evolution that involves interferences associated with the time dependence of the coupling terms and the energy phases such as $\exp[i\int_t^\tau dx(\varepsilon_{\vec{k}} - \varepsilon_{1s})]$ [see Eqs. (12) and (13)], (A1)–(A8). In Fig. 12 the contributions to the ion neutralization provided by the ground and excited channels are shown as a function of the ion trajectory for an incoming energy of 3 keV. The results are obtained by including the four nearest C atoms. In this figure we compare the contributions of the ground state obtained from the different calculations: spinless, including spin statistics, and considering the excited configurations. The spinless case was discussed previously in Sec. III A1: Electron loss in the region close to the surfaceoccurrs due to the large coupling between the He-1s and the C states that allows for promoting the electron to empty band states. The spin statistic effect does not change this scenario, while the presence of excited configurations gives to the ionization level the possibility of a resonant electron capture at distances close to the surface.

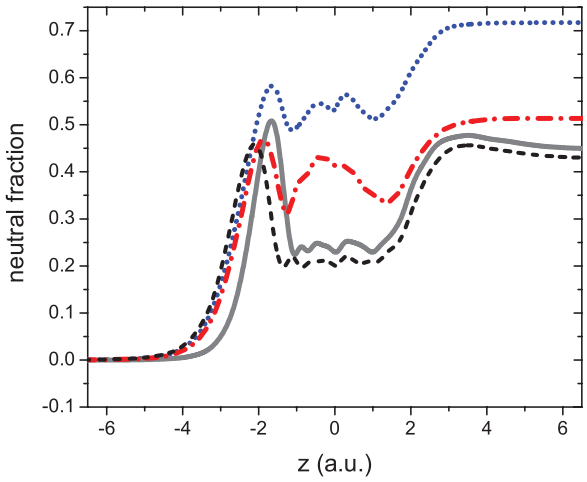

FIG. 12. (Color online) The contribution of the ground state to the neutral fraction as a function of the distance to the surface for $E_{\mathrm{in}} =$ 3 keV: spinless calculation (gray line), by including spin statistic effects (dashed line), by considering the excited $(1s2s)$ configuration (dash-dotted line), and by considering both the $(1s2s)$ and the $(1s2p)$ excited configurations (dotted line).

IV. CONCLUSIONS

We performed a time-dependent quantum mechanical calculation of the charge exchange process in He^+/HOPG collision, by considering the resonant neutralization to the ground and first excited states of the He atom. The possibility of many states in the atom is taken into account by an extended atomic Hamiltonian that allows us to perform a time-dependent interaction of configurations. This robust theoretical proposal means a clear improvement of the very approximated treatment of Ref. 26. The Anderson Hamiltonian is projected on the energetically favorable electronic configurations of the helium atom and the occupations of these atomic configurations are calculated by using appropriate Green functions solved by the equation of motion method. Our results reproduce the very high neutral fractions measured in He^+ scattered by HOPG at intermediate incoming energies only when excited configurations $(1s2s)$ and $(1s2p)$ are considered in the atom-surface interaction. It is found that the correlation effects act in order to increase the neutralization to the ground state, and it is explained in terms of the energy level shift produced by the interaction between atom excited states and the surface band states. The contribution to the ground state occupation due to Auger deexcitation of the excited states is not negligible, and the AN process is expected to contribute in the range of small energy values where, according to our results, the resonant process alone cannot justify a complete ion neutralization.

ACKNOWLEDGMENTS

This work was supported by ANPCyT through PICT-2007-00811 and 2010-0294, and by U.N.L. through CAI + D grants.

APPENDIX: TIME EVOLUTION OF GREEN FUNCTIONS $G_{|A\rangle\langle B|}(t,t')$ AND $F_{|A\rangle\langle B|}(t,t')$, WITH $A = 1s\uparrow 2\alpha\sigma$ AND $B = 1s\uparrow$

By following the same procedure of Sec. II C, we arrive at the expressions:

$$
\begin{aligned}
&i\frac{d}{dt}g_{|A\rangle\langle B|}(t,t') \\
&= \delta(t-t')\langle|[|1s\uparrow 2\alpha\sigma\rangle\langle 1s\uparrow 2\alpha\sigma| + |1s\uparrow\rangle\langle 1s\uparrow|]|\rangle + i\sum_{\vec{k}}\Bigg[-\tilde{V}^{*}_{\vec{k}1s}(t)\langle|1s\uparrow 1s\downarrow\rangle\langle 1s\downarrow|\hat{c}^{\dagger}_{\vec{k}\uparrow}\rangle_{t'}\exp\left(i\int_{t'}^{t}\varepsilon_{1s}\,dx\right) \\
&\quad + \sum_{\substack{\sigma',\beta=s,p;\\ \beta\alpha'\neq\alpha\sigma}}\hat{V}^{*}_{\vec{k}2\beta}(t)\langle|1s\uparrow 2\beta\sigma'\rangle\langle 1s\uparrow|\hat{c}^{\dagger}_{\vec{k}\sigma'}\rangle_{t'}\exp\left(i\int_{t'}^{t}\varepsilon_{2\beta\sigma}\,dx\right)\Bigg]e^{-i\varepsilon_{\vec{k}}(t-t')} + \int_{-\infty}^{\infty}d\tau\Bigg\{\Xi^{0}_{2\alpha}(t,\tau)\exp\left(-i\int_{t}^{\tau}\varepsilon_{2\alpha\sigma}\,dx\right) \\
&\quad + \Xi^{<}_{1s,\downarrow}(t,\tau)\exp\left(-i\int_{t}^{\tau}\varepsilon_{1s}dx\right) + \sum_{\substack{\sigma',\beta=s,p;\\ \beta\sigma'\neq\alpha\sigma}}\Xi^{<}_{2\beta,\sigma'}(t,\tau)\exp\left(-i\int_{t}^{\tau}\varepsilon_{2\beta\sigma}dx\right)\Bigg\}g_{|A\rangle\langle B|}(\tau,t') \qquad \text{(A1)}
\end{aligned}
$$

$$
\begin{aligned}
i\frac{d}{dt}f_{|A\rangle\langle B|}(t,t') &= i\sum_{\vec{k}}\Bigg[-\langle 2n_{\vec{k}\downarrow}-1\rangle\tilde{V}^{*}_{\vec{k}1s}(t)\langle|1s\uparrow 1s\downarrow\rangle\langle 1s\downarrow|\hat{c}^{\dagger}_{\vec{k}\uparrow}\rangle_{t'}\exp\left(i\int_{t'}^{t}\varepsilon_{1s}\,dx\right) \\
&\quad + \sum_{\substack{\sigma',\beta=s,p;\\ \beta\alpha'\neq\alpha\sigma}}\langle 2n_{\vec{k}\sigma'}-1\rangle\hat{V}^{*}_{\vec{k}2\beta}(t)\langle|1s\uparrow 2\beta\sigma'\rangle\langle 1s\uparrow|\hat{c}^{\dagger}_{\vec{k}\sigma'}\rangle_{t'}\exp\left(i\int_{t'}^{t}\varepsilon_{2\beta\sigma}\,dx\right)\Bigg]e^{-i\varepsilon_{\vec{k}}(t-t')} \\
&\quad + \int_{-\infty}^{\infty}d\tau\Bigg\{\Xi^{0,R}_{2\alpha}(t,\tau)\exp\left(-i\int_{t}^{\tau}\varepsilon_{2\alpha\sigma}\,dx\right) + \Xi^{<R}_{1s,\downarrow}(t,\tau)\exp\left(-i\int_{t}^{\tau}\varepsilon_{1s}\,dx\right) \\
&\quad + \sum_{\substack{\sigma',\beta=s,p;\\ \beta\sigma'\neq\alpha\sigma}}\Xi^{<,R}_{2\beta,\sigma'}(t,\tau)\exp\left(-i\int_{t}^{\tau}\varepsilon_{2\beta\sigma}\,dx\right)\Bigg\}f_{|A\rangle\langle B|}(\tau,t') + \int_{-\infty}^{\infty}d\tau\Bigg\{\Omega^{0}_{2\alpha}(t,\tau)\exp\left(-i\int_{t}^{\tau}\varepsilon_{2\alpha\sigma}\,dx\right) \\
&\quad + \Omega^{<}_{1s,\downarrow}(t,\tau)\exp\left(-i\int_{t}^{\tau}\varepsilon_{1s}\,dx\right) + \sum_{\substack{\sigma',\beta=s,p;\\ \beta\sigma'\neq\alpha\sigma}}\Omega^{<}_{2\beta,\sigma'}(t,\tau)\exp\left(-i\int_{t}^{\tau}\varepsilon_{2\beta\sigma}\,dx\right)\Bigg\}g_{|A\rangle\langle B|}(\tau,t'). \qquad \text{(A2)}
\end{aligned}
$$

The following self-energies were introduced in Eqs. (12), (13), (A1), and (A2):

$$\Xi_i^0(t,\tau) = i\Theta(\tau - t)\sum_{\vec{k}} \hat{V}^*_{\vec{k}i}(t)\hat{V}_{\vec{k}i}(\tau)e^{-i\varepsilon_{\vec{k}}(t-\tau)} = \left[\Xi_i^{0,R}(\tau,t)\right]^*, \tag{A3}$$

$$\Omega^0_{i,\sigma}(t,\tau) = -i\sum_{\vec{k}} \langle 2n_{\vec{k}\sigma} - 1\rangle V^*_{\vec{k}i}(t)V_{\vec{k}i}(\tau)e^{-i\varepsilon_{\vec{k}}(t-\tau)}, \tag{A4}$$

$$\Xi^>_{1s\sigma}(t,\tau) = i\Theta(\tau - t)\sum_{\vec{k}} \tilde{V}^*_{\vec{k}1s}(t)\tilde{V}_{\vec{k}1s}(\tau)\langle 1 - n_{\vec{k}\sigma}\rangle e^{-i\varepsilon_{\vec{k}}(t-\tau)} = \left[\Xi^{>,R}_{1s\sigma}(\tau,t)\right]^*, \tag{A5}$$

$$\Omega^>_{1s\sigma}(t,\tau) = -i\sum_{\vec{k}} \langle 2n_{\vec{k}\sigma} - 1\rangle \tilde{V}^*_{\vec{k}1s}(t)\tilde{V}_{\vec{k}1s}(\tau) \times \langle 1 - n_{\vec{k}\sigma}\rangle e^{-i\varepsilon_{\vec{k}}(t-\tau)}, \tag{A6}$$

$$\Xi^<_{i\sigma}(t,\tau) = i\Theta(\tau - t)\sum_{\vec{k}} \hat{V}^*_{\vec{k}i}(t)\hat{V}_{\vec{k}i}(\tau)\langle n_{\vec{k}\sigma}\rangle e^{-i\varepsilon_{\vec{k}}(t-\tau)} = \left[\Xi^{<,R}_{i\sigma}(\tau,t)\right]^*, \tag{A7}$$

$$\Omega^<_{i\sigma}(t,\tau) = -i\sum_{\vec{k}} \langle 2n_{\vec{k}\sigma} - 1\rangle \hat{V}^*_{\vec{k}i}(t)\hat{V}_{\vec{k}i}(\tau)\langle n_{\vec{k}\sigma}\rangle e^{-i\varepsilon_{\vec{k}}(t-\tau)}. \tag{A8}$$

In Eqs. (A1)–(A8), $\langle \hat{n}_{\vec{k}\sigma}\rangle$ is given by the Fermi function at a temperature T.

[1] H. H. Brongersma, M. Draxler, M. de Ridder, and P. Bauer, Surf. Sci. Rep. **62**, 63 (2007).
[2] A. Blandin, A. Nourtier, and D. Hone, J. Physique **37**, 369 (1976).
[3] R. Brako and D. M. Newns, Surf. Sci. **108**, 253 (1981).
[4] J. J. C. Geerlings and J. Los, Phys. Rep. **190**, 133 (1990).
[5] J. Merino and J. B. Marston, Phys. Rev. B **58**, 6982 (1998).
[6] A. G. Borisov, A. K. Kazansky, and J. P. Gauyacq, Phys. Rev. B **59**, 10935 (1999).
[7] A. G. Borisov, D. Teillet-Billy, and J. P. Gauyacq, Phys. Rev. Lett. **68**, 2842 (1992)
[8] J. B. Marston, D. R. Andersson, E. R. Behringer, B. H. Cooper, C. A. DiRubio, G. A. Kimmel, and C. Richardson, Phys. Rev. B **48**, 7809 (1993).
[9] P. Kurpick, U. Thumm, and U. Wille, Phys. Rev. A **56**, 543 (1997).
[10] H. D. Hagstrum, Phys. Rev. **96**, 336 (1954).
[11] R. A. Baragiola and C. A. Dukes, Phys. Rev. Lett. **76**, 2547 (1996).
[12] M. A. Cazalilla, N. Lorente, R. D. Muiño, J.-P. Gauyacq, D. Teillet-Billy, and P. M. Echenique, Phys. Rev. B **58**, 13991 (1998).
[13] M. Alducin, J. I. Juaristi, R. Díez Muiño, M. Rösler, and P. M. Echenique, Phys. Rev. A **72**, 024901 (2005).
[14] Y. Bandurin, V. A. Esaulov, L. Guillemot, and R. C. Monreal, Phys. Rev. Lett. **92**, 017601 (2004).
[15] D. Valdes, E. C. Goldberg, J. M. Blanco, and R. C. Monreal, Phys. Rev. B **71**, 245417 (2005).
[16] D. Goebl, D. Valdés, E. Abad, R. C. Monreal, D. Primetzhofer, and P. Bauer, Phys. Rev. B **84**, 165428 (2011).
[17] R. Monreal and N. Lorente, Phys. Rev. B **52**, 4760 (1995).
[18] N. Lorente, R. C. Monreal, and M. Alducin, Phys. Rev. A **49**, 4716 (1994).
[19] M. Alducin, Phys. Rev. A **53**, 4222 (1996).
[20] N. Bajales, J. Ferrón, and E. C. Goldberg, Phys. Rev. B **76**, 245431 (2007).
[21] S. Tsuneyuki and M. Tsukada, Phys. Rev. B **34**, 5758 (1986).
[22] E. C. Goldberg, R. Monreal, F. Flores, H. H. Brongersma, and P. Bauer, Surf. Sci. **440**, L875 (1999).
[23] N. P. Wang, E. A. García, R. Monreal, F. Flores, E. C. Goldberg, H. H. Brongersma, and P. Bauer, Phys. Rev. A **64**, 012901 (2001).
[24] S. N. Mikhailov, R. J. M. Elfrink, J. P. Jacobs, L. C. A. van den Oetelaar, P. J. Scanlon, and H. H. Brongersma, Nucl. Instrum. Methods Phys. Res. B **93**, 210 (1994).
[25] R. Souda and K. Yamamoto, Nucl. Instrum. Methods Phys. Res. B **125**, 256 (1997).
[26] N. B. Luna, F. J. Bonetto, R. A. Vidal, E. C. Goldberg, and J. Ferrón, J. Mol. Catal. A: Chem. **281**, 237 (2008).
[27] R. Cortenraad, A. W. Denier van der Gon, H. H. Brongersma, S. N. Ermolov, and V. G. Glebovsky, Phys. Rev. B **65**, 195414 (2002).
[28] J. C. Lancaster, F. J. Kontur, G. K. Walters, and F. B. Dunning, Phys. Rev. B **67**, 115413 (2003).
[29] S. Wethekam and H. Winter, Surf. Sci. **596**, L319 (2005).
[30] E. C. Goldberg, F. Flores, and R. C. Monreal, Phys. Rev. B **71**, 035112 (2005).
[31] L. V. Keldysh, Zh. Eksp. Teor. Fiz. **47**, 1515 (1964).
[32] L. V. Keldysh, Sov. Phys. JETP **20**, 1018 (1965).
[33] P. W. Anderson, Phys. Rev. **124**, 41 (1961).
[34] P. G. Bolcatto, E. C. Goldberg, and M. C. G. Passeggi, Phys. Rev. B **58**, 5007 (1998).
[35] P. O. Lowdin, J. Chem. Phys. **18**, 365 (1950).
[36] S. Huzinaga, J. Andzelm, M. Klobukowsky, E. Radzio-Andzelm, Y. Sakai, and H. Tatewaki, *Gaussian Basis Set for Molecular Calculation* (Elsevier, Amsterdam, 1984).
[37] S. Huzinaga, J. Chem. Phys. **42**, 1293 (1965).
[38] A. A. Radzig and B. M. Smirnov, *Reference Data on Atoms, Molecules, and Ions*, Springer Series in Chemical Physics Vol. 31 (Springer-Verlag, Berlin, 1985).
[39] J. P. Lewis, K. R. Glaesemann, G. A. Voth, J. Fritsch, A. A. Demkov, J. Ortega, and O. F. Sankey, Phys. Rev. B **64**, 195103 (2001).

[40]P. Jelinek, H. Wang, J. P. Lewis, O. F. Sankey, and J. Ortega, Phys. Rev. B **71**, 235101 (2005).
[41]F. Bonetto, M. A. Romero, E. A. García, R. Vidal, J. Ferrón, and E. C. Goldberg, Europhys. Lett. **80**, 53002 (2007).
[42]H. Shao, D. C. Langreth, and P. Nordlander, Phys. Rev. B **49**, 13929 (1994).
[43]J. Merino and J. B. Marston, Phys. Rev. B **69**, 115304 (2004).
[44]H. Shao, P. Nordlander, and D. C. Langreth, Phys. Rev. Lett. **77**, 948 (1996).
[45]F. Bonetto, M. A. Romero, E. A. García, R. A. Vidal, J. Ferrón, and E. C. Goldberg, Phys. Rev. B **78**, 075422 (2008).